HHS Public Access

Author manuscript

Ann Biomed Eng. Author manuscript; available in PMC 2016 November 01.

Published in final edited form as:

Ann Biomed Eng. 2015 November ; 43(11): 2618–2629. doi:10.1007/s10439-015-1337-0.

Reinforcement of mono- and bi-layer poly(ethylene glycol) hydrogels with a fibrous collagen scaffold

K. R. C. Kinneberg[1], **A. Nelson**[2], **M. Stender**[1], **A. H. Aziz**[2,3], **L. C. Mozdzen**[4], **B. A. C. Harley**[4], **S. J. Bryant**[2,3,5], and **V. L. Ferguson**[1,3,5,*]

[1]Department of Mechanical Engineering, University of Colorado

[2]Department of Chemical and Biological Engineering, University of Colorado

[3]BioFrontiers Institute, University of Colorado

[4]Department of Chemical and Biomolecular Engineering, University of Illinois at Urbana-Champaign

[5]Material Science & Engineering Program, University of Colorado

Abstract

Biomaterial-based tissue engineering strategies hold great promise for osteochondral tissue repair. Yet significant challenges remain in joining highly dissimilar materials to achieve a biomimetic, mechanically robust design for repairing interfaces between soft tissue and bone. This study sought to improve interfacial properties and function in a bilayer, multi-phase hydrogel interpenetrated with a fibrous collagen scaffold. ‘Soft’ 10% (w/w) and ‘stiff’ 30% (w/w) PEGDM was formed into mono- or bilayer hydrogels possessing a sharp diffusional interface. Hydrogels were evaluated as single- (hydrogel only) or multi-phase (hydrogel+fibrous scaffold penetrating throughout the stiff layer and extending >500μm into the soft layer). Including a fibrous scaffold into both soft and stiff single-phase hydrogels significantly increased tangent modulus and toughness and decreased lateral expansion under compressive loading. In multi-phase hydrogels, finite element simulations predict substantially reduced stress and strain gradients across the soft—stiff hydrogel interface. When combining two low moduli constituent material, composites theory poorly predicts the observed, large modulus increases. These results suggest material structure associated with the fibrous scaffold penetrating within the PEG hydrogel as the major contributor to improved properties and function – the hydrogel bore compressive loads and the 3D fibrous scaffold was loaded in tension thus resisting lateral expansion.

Keywords

Mechanical properties; tissue engineering; osteochondral; interface; hydrogel; scaffold; multi-phase

*Corresponding author: Virginia L. Ferguson, 1111 Engineering Drive; UCB 427, Department of Mechanical Engineering, University of Colorado, Boulder, CO 80309 USA, virginia.ferguson@colorado.edu Telephone: 1-303-735-5232, Fax: 1-303-492-3498.

Introduction

Many interfacial tissues in the musculoskeletal system act as junctions that enable efficient transfer of mechanical loads from one tissue to another. One such interface exists between bone and cartilage, which can be found in both articulating joints and the spine. This interface, which is relatively thin at ≤100's of microns,[1] anchors together stiff subchondral bone and compliant hyaline cartilage. While there is an abrupt change in modulus of ∼4 orders of magnitude across this interface when progressing from bone to cartilage,[10] tissues proximal to this interface rarely fail *in vivo.* This observation is attributed in large part to the structural organization of the tissue. In particular, collagen fibers extend from the mineral tidemark at the interface into the deep zone of hyaline cartilage. Glycosaminoglycans, through their fixed negative charges, trap water in interstitial spaces within the cartilage and impart resistance to compression by charge-charge repulsion and interstitial fluid pressurization. As loads are transferred through the tissue, the collagen fibrils are thought to dissipate forces,[39] thus minimizing the effects of stress concentration at the interface. The unique composition and architecture of the osteochondral interface are critical components to the overall function of the bone-cartilage interface and ultimately protects the tissue from mechanical failure.

Scaffold-based tissue engineering approaches are promising for treating lesions that span cartilage, bone and the osteochondral interface. Given the distinct compositions and mechanical properties of cartilage and bone, multi-phasic scaffolds, *i.e.*, composites consisting of two or more distinct materials[41], have been developed where one phase is designed for bone regeneration and another phase for cartilage regeneration.[31, 32, 36, 49] The most common scaffold designs include a stiff porous ceramic scaffold for the bone region topped with a soft polymeric phase[15, 20, 27] for the cartilage region, or in some cases both phases are made from soft polymers.[16, 21, 28, 29, 37, 40, 48, 54] However, without a secure linkage between the two phases, delamination at the interface can occur[48] and *in vivo* the cartilage layer is prone to shearing.[30] To overcome this shortcoming, methods to produce continuous gradients across two adjacent layered phases have been developed. For example, interdiffusion between the two phases prior to processing leads to a continuous interface possessing the compositional make-up of both phases.[24, 55] Templating methods have also been developed to create an abrupt change in pore size, where the polymer phase is continuous across the entire scaffold.[19] Overall, these studies point towards the need for a mechanically robust interface in biphasic scaffolds, particularly when mechanical loads are present and the two, layered phases possess substantially different mechanical properties.

The goal of this study was to investigate a biomimetic design for reinforcing interfaces between hydrogel-based biomaterials, in this case based on poly(ethylene glycol) (PEG) hydrogels. PEG hydrogels were chosen for their promise in cartilage[46, 47], bone[4, 53], and osteochondral[50] tissue engineering and the ability to achieve a range of mechanical properties that are suitable for cell encapsulation.[2, 42, 52] We hypothesized that incorporating a fibrous, collagen network, previously characterized for mechanical properties and structure[23] and cytocompatibility[7, 8, 17, 26, 33, 58], into a PEG hydrogel would improve the overall mechanical properties, specifically by resisting lateral expansion, improving the compressive modulus, and enhancing toughness. To test this hypothesis, a cytocompatible

and low-density open-cell foam scaffold prepared from collagen and glycosaminoglycans[5-7, 26, 38] was incorporated into mono-and bi-layer PEG hydrogels formed from monomers of PEG dimethacrylate (PEGDM). While Type II collagen dominates in native cartilage, fibrous scaffolds consisting predominately of Type I collagen were used as a proof-of-concept due to our extensive, prior characterization of these materials (note that these same materials were termed “collagen-GAG scaffolds” in prior works)[23, 24, 38, 56, 59]. In the present study, four material systems were fabricated as follows (Figure 1): (1) single-phase, mono-layer hydrogels were composed of either soft or stiff PEG hydrogels; (2) single-phase, bi-layer hydrogels were formed with a stiff hydrogel layered onto a soft hydrogel of equal dimensions; (3) multi-phase, mono-layer hydrogels were formed by incorporating the fibrous collagen scaffold network throughout mono-layer hydrogels; and (4) multi-phase, bilayer hydrogels were formed by incorporating the fibrous collagen scaffold network such that fibers persisted throughout the stiff layer and extended across the interface into the soft hydrogel, but did not extend appreciably into the bulk of the soft layer to mimic the physical construction of the osteochondral interface. The four constructs generated for this study were characterized experimentally through microscopy and unconfined compression mechanical testing and modeled using finite element analysis.

Materials and Methods

Methacrylation of PEG

PEG (3000 molecular weight (MW); Sigma-Aldrich, St. Louis, MO) was reacted with methacrylic anhydride (10 mol per mol PEG; Sigma-Aldrich) with trace amounts of hydroquinone (Sigma-Aldrich) following a microwave methacrylation protocol, as previously described.[35] The product PEGDM was purified by precipitation in ethyl ether and dried under vacuum for 2 days. The final product was determined to be 89% methacrylated via ^{1}H NMR (Varian INOVA 500) by comparing the area under the integral for the vinyl resonances to the methylene protons in the PEG backbone.

Fabrication of fibrous scaffolds

Cytocompatible[7, 8, 17, 26, 33, 58], fibrous scaffolds comprised of collagen and glycosaminoglycans (GAG) were fabricated via a lyophilization process described previously.[38] Briefly, type I collagen isolated from bovine tendon (1.0 wt %; Sigma-Aldrich) was solubilized in 0.05 M acetic acid and co-precipitated with GAG (chondroitin-6-sulfate isolated from shark cartilage, 0.1 wt%; Sigma-Aldrich) during homogenization. Using a constant cooling rate technique,[43, 44] the collagen and GAG suspension was reduced in temperature from 20 °C to -10 °C (mean pore size 151 (32) μm, mean (SD))[23] and lyophilized. Scaffolds were physically crosslinked through a dehydrothermal-based (DHT) process in which scaffolds were placed in a vacuum oven (Fisher IsoTemp 201, Fisher Scientific, Boston, MA) under a 50 mTorr vacuum.[43, 44, 58] Cylindrical fibrous scaffolds were cored using a 5 mm biopsy punch and then soaked in 100% ethanol for 24 hours, followed by several rinses in deionized water (diH_2O) overnight. Scaffolds were further crosslinked (room temperature for 1.5 hours) in a solution of 1-ethyl-3-[3-dimethylaminopropyl] carbodiimide hydrochloride (EDC) (Sigma Aldrich) and N-hydroxysulfosuccinimide (NHS) (Sigma Aldrich) at a molar ratio of 5:2:1

EDC:NHS:COOH.[23, 51]. The fibrous scaffolds were rinsed several times in diH_2O before use.

Fabrication of PEG hydrogels

PEG hydrogels were formed in 1 mL syringes by polymerizing a precursor solution containing either 10% (w/w) PEGDM or 30% (w/w) PEGDM in the presence of a photoinitiator (2-hydroxy-4′-(2-hydroxyethoxy)-2-methylpropiophenone, 0.05% (w/w); Irgacure 2959; BASF) in diH_2O under 352 nm light (UVP model XX-20) at ∼5 mW/cm^2. Single phase, mono-layer hydrogels with cylindrical dimensions of ∼5 mm diameter and ∼5 mm height were produced by polymerizing for 10 minutes. Single-phase, bi-layer PEG hydrogels with dimensions of ∼5 mm diameter (*i.e.*, the inner diameter of the syringe) and ∼5 mm height were made by first polymerizing 45 μl of 30% PEGDM for 7 minutes and then adding a second layer of 45 ul of 10% PEGDM and immediately polymerizing for an additional 10 minutes. To produce multiphase, mono-layer hydrogels, fibrous scaffolds were incorporated into mono-layer hydrogels by removing excess water from the scaffold, submerging in 50 μl of the precursor solution, exposing to three consecutive 4 second vacuum/release cycles, and finally removing excess polymer solution. The fibrous scaffold with the infiltrated precursor solution was polymerized for 10 minutes. For multi-phase, bi-layer hydrogels, 30 μl of 30% PEGDM precursor solution was added to each fibrous scaffold as described above before being polymerized for 7 minutes. Then, an additional 45 μl of 10% PEGDM precursor solution was added and the layered composite material was polymerized for an additional 10 minutes. All hydrogels were stored in diH_2O for at least 48 hours to reach equilibrium swelling before mechanical testing.

Scanning Electron Microscopy

Scaffold microstructure was visualized using scanning electron microscopy (SEM) using a JEOL JSM-6060LV Low Vacuum Scanning Electron Microscope (JEOL USA, Peabody, MA). Images were collected using a standard secondary electron detector under low vacuum, bypassing the need for any sample sputter coating steps.[24]

Confocal microscopy and interfacial thickness

Fluorescently labeled hydrogels were formed by incorporating fluorophores into each precursor solution. In brief, 0.01 mM Alexa Fluor® 488 C5 Maleimide was added to the 30% PEGDM precursor solution and 0.01 mM methacryloxyethyl thiocarbamoyl rhodamine B was added to the 10% PEGDM solution. To enable visualization and quantification of the single phase, bi-layer hydrogels (*i.e.*, without the fibrous scaffold), hydrogels were fabricated between two glass slides in silicon molds of dimensions 10 mm wide by 2 mm thick resulting in gels with a total height of ∼5 mm. Hydrogels were imaged by confocal microscopy. Interface thickness was determined from confocal images by generating a line perpendicular to the interface. Using ImageJ software analysis tools, intensity as a function of distance across the interface was plotted for each of the fluorophore channels. The interface thickness was denoted by the total distance across which both fluorophore channels detected fluorescence signal over the background. To evaluate the position of the fibrous scaffold within multi-phase hydrogels, a Zeiss510/META laser scanning, two-photon

confocal microscope (Carl Zeiss, Thornwood, NY), with a Zeiss Plan Neofluar 25×/0.80 Imm Korr objective was used to image autofluorescent collagen. This technique enabled visualization of the fibrous collagen scaffold network within the fluorescently labeled soft and stiff phases; images were added to enable visualization of the multiple phases *in situ*.

Mechanical testing of PEG hydrogels

Compressive testing was conducted on a Mechanical Testing System (MTS; Eden Prairie, MN). Equilibrium swollen hydrogels (n = 5 / group) were tested in unconfined compression at a constant strain rate of 0.5 mm/min to 40% strain (1.5 mN pre-load; limited by a 4 N max load with a total load cell capacity of 5 N). Testing fixtures were well lubricated to minimize friction at sites of sample contact. The tangent elastic modulus was calculated from the tangent curve to each portion of the stress-strain curve spanning successive 5% strain increments between 10 to 35%. For both single- and multi-phase, monolayer hydrogels, toughness was calculated as the area under each stress-strain curve to 20% strain in the stiff hydrogels and to 35% strain in the soft hydrogels. The selection of these endpoint values for evaluating toughness were based on the maximum loads achieved in compression testing and could have easily instead been evaluated at a single value of strain. Digital photographs were collected of the single-phase and multi-phase, mono-layer hydrogels at 0 % and 40% strain, calibrated for distance, and analyzed using NIH ImageJ software to determine the longitudinal and lateral expansion. Lateral expansion was calculated as:

$$Lateral\ Expansion = -\varepsilon_{lateral}/\varepsilon_{longitudinal} \quad (1)$$

where ε is calculated as engineering strain (*i.e.*, change in length / initial length). Hydrogels behave non-linearly when subjected to large strains (*e.g.*, 40% strain), thus equation (1) shows a calculation that is consistent with Poisson's ratio yet is instead described here as “Lateral Expansion” to indicate a departure from linear elastic behavior.

Finite Element Simulations

Two bi-layer PEG hydrogels were modeled using 2-D axisymmetric finite element models of unconfined compression developed in Abaqus v6.13 (Simulia). Bi-layer, single-phase materials included soft, 10% PEG hydrogel stacked superior to the stiff, 30% PEG hydrogel. Bi-layer, multi-phase materials simulated a fibrous scaffold that was distributed throughout the 30% PEG hydrogel and that also penetrated 500 micrometers into the overlying 10% PEG layer. Both models simulated cylindrical hydrogel samples with a radius of 2.5 mm and a height of 5.0 mm using 338 bilinear axisymmetric quadrilateral elements with full integration. For both models, the soft and stiff regions were assumed to be 2.5 mm high. Displacements were disallowed in a direction perpendicular to the axis of rotation, and the top surface was constrained against a rigid fixed platen using a frictionless surface-to-surface contact algorithm. To simulate loading, a displacement boundary condition was applied to the bottom surface resulting in a 20% compressive strain on the sample. The outer radial boundary was unconstrained. Adjacent differential material regions were joined using a tied contact constraint. All materials were assumed to be nonlinear elastic with compressive modulus values obtained from the tangent modulus measures collected for

single-phase materials in this study (Fig. 3). Poisson's ratios for the 30% PEG stiff hydrogel with and without inclusion of the fibrous scaffold were assumed based on experimental results for lateral expansion as 0.14 and 0.21, respectively. For the 10% PEG soft hydrogel, due to the theoretical upper limit of 0.5 for isotropic materials a Poisson's ratio of 0.49 was assumed and reduced to 0.40 with the inclusion of the fibrous scaffold based on experimental results that showed a reduction in lateral expansion with the inclusion of the fibrous scaffold for the 10% PEG soft hydrogel.

Statistical analysis

Data were normal and homoscedastic. Significant differences were established using a multivariate ANOVA. Significance was assigned at $p < 0.05$. Post-hoc comparisons were performed using Fisher's protected LSD. All data are presented as mean with standard deviation.

Results

Four hydrogel conditions were investigated in this study (see experimental set-up, Fig. 1), which included mono- and bi-layer PEG hydrogels formed as a single-phase material (*i.e.*, no fibrous scaffold) and as multi-phase materials containing a cytocompatible fibrous scaffold. In multi-phase, mono-layer materials, the scaffold interpenetrated throughout the entire volume of each soft 10% (w/w) and stiff 30%, hydrogel monolayer. In the multi-phase materials, the scaffold interpenetrated throughout the entire height of the stiff hydrogel and approximately 500 - 1000 μm into the soft hydrogel (Fig. 2E). Qualitatively, SEM images of the fibrous scaffold (Fig. 2) reveal a high degree of regular, connected pores within a continuous network of fibers (mean pore size of 150 μm, porosity of ∼99%). In single-phase, bi-layer hydrogels, a relatively thin and abrupt interface was formed between the soft and stiff hydrogel layers. This interface contained a thin layer formed by diffusion of the two hydrogels that was measured to be 74 (16) μm thick, a value that corresponds to approximately 1.5% of the total height of the hydrogel (Fig. 2). When the fibrous scaffold was incorporated into the multi-phase bi-layered hydrogels, confocal microscopy with SHG was used to confirm: (1) that the fibrous scaffold extended across the interface and into the soft hydrogel layer and (2) that the hydrogel evenly penetrated the pore spaces within the fibrous scaffold (Fig. 2). Analysis of the resulting confocal images showed excellent infiltration of the hydrogel into pores, where some regions shown in Fig 2E appear dark only due to artifacts produced during image processing to create the composite figure.

In mono-layer hydrogels, the stiff, 30 % (w/w), hydrogel possessed significantly greater tangent moduli than the soft, 10 % (w/w), hydrogel (Fig. 3). As an example, between 10-15% strain, the soft hydrogel samples produced a tangent modulus of 131 (5.9) kPa compared to the stiff hydrogel tangent modulus of 877 (34.5) kPa. For both soft and stiff mono-layer hydrogels, the tangent modulus was significantly greater across all strain levels ($p < 0.001$ for all comparisons) in the multi-phase hydrogels, that contained the fibrous scaffold, when compared to the single-phase hydrogels. For the soft hydrogels, inclusion of the fibrous scaffold increased tangent moduli by 34.3 % when evaluated at 15 – 20 % strain and by 53.0 % at 30 – 35 % strain. Although the stiff hydrogels were only compressed to

20% strain (again, due to limitations of our mechanical testing setup), the fibrous scaffold significantly increased the tangent modulus by ∼10%. The toughness, measured as the area under each stress-strain curve to 20% strain in the stiff hydrogels and to 35% strain in the soft hydrogels, increased with inclusion of the fibrous scaffold by 17.6 % and 41.9 % for stiff and soft hydrogels, respectively ($p < 0.001$). A table insert within Figure 3 lists the mean and SD values for toughness. Incorporating a fibrous scaffold into mono-layer hydrogels revealed that significantly greater lateral expansion occurred in the single-phase soft hydrogel (at ∼0.6 mm/mm) as compared to the single-phase stiff hydrogel (at ∼0.2 mm/mm) (Fig. 4). Moreover, inclusion of the fibrous scaffold reduced lateral expansion by 12% ($p = 0.07$) in the soft hydrogel and more significantly in the stiff hydrogel by 33% ($p = 0.02$).

The mechanical properties of the bi-layer hydrogels as single- or multi-phase materials were also assessed. At each strain increment evaluated, tangent moduli of single-phase bi-layer hydrogels (Fig 5) were greater than the tangent moduli reported in Figure 3 for the soft single-phase, mono-layer hydrogels and lower than the tangent moduli of the stiff hydrogels. For example at 10-15% strain, the tangent modulus of the single-phase, bi-layer hydrogel was 319 kPa, which falls in between the soft and stiff single-phase, mono-layer hydrogels (131 kPa and 877 kPa, respectively). The inclusion of the fibrous scaffold into bi-layer hydrogels did not significantly affect the tangent modulus across all strain levels evaluated. Under compressive strain applied to the bi-layer hydrogels, the soft layer experienced high lateral expansion as shown in the representative image in Fig. 5. However, in bi-layer materials, the degree of lateral expansion was highly non-uniform and thus was difficult to consistently quantify. As also illustrated in Fig. 5, the smallest lateral expansion in a bi-layer hydrogel consistently occurred at the interface between the soft and stiff hydrogel layers. Hydrogel dimensions during lateral expansion increased with distance into the soft hydrogel and away from the interface with the highest lateral expansion being at the top of soft layer.

Finite element simulations demonstrated that the addition of the fibrous scaffold to form multi-phase hydrogels resulted in an overall improvement in the stress and strain profile in the bi-layer hydrogels (Fig. 6). Tensile strains develop within both soft and stiff layers that lie along a direction oriented ∼ 45° from the interface in single-phase constructs (Fig. 6 A,B). Inclusion of the fibrous scaffold mitigates these tensile strains, where stress contours illustrate a more graded strain field throughout with reduced strain magnitudes and concentrations at the interface. Similarly, principal stresses (Fig. 6 C,D) and shear strains (Fig. 6 E,F) are of smaller magnitude and distributed more evenly in multi-phase, bi-layer scaffolds. Finally, displacement in the lateral (*i.e.*, horizontal) direction and away from the center axis of the axisymmetric model were reduced in the region of the bi-layer hydrogel near the interface between the soft and stiff phases within multi-phase materials (Fig. 6 G,H). This lateral displacement was localized within the soft hydrogel for both single- and multi-phase cases, where a notable reduction in bulging of the soft layer occurred in multi-phase scaffolds.

Discussion

In this study, we demonstrate that the inclusion of a porous and fibrous collagenous scaffold within a PEG hydrogel, consisting of two dissimilar layers, improves overall mechanical properties and interfacial behavior. For mono-layers of hydrogel, those containing the fibrous scaffold exhibited significantly increased tangent modulus, increased toughness, and reduced lateral expansion. For bi-layer hydrogels consisting of soft and stiff layers, finite element analysis demonstrated that inclusion of the fibrous scaffold across the interface contributed to a more gradual strain gradient across the relatively abrupt interface between the two dissimilar hydrogel materials. Overall, the fibrous scaffold serves to improve mechanical function within PEG hydrogels and captures some of the key characteristics of collagen fibers within the native osteochondral tissues.

The fibrous scaffold employed in this study possesses relatively poor mechanical properties, yet its inclusion made a significant contribution to mechanical behavior. These fibrous collagen scaffold networks are highly porous (*e.g.*, possess a mean pore size of 150 μm and porosity of ∼99%) and have a low compressive modulus (*i.e.*, ∼1.5 kPa in the hydrated state)[23] The single-phase PEG hydrogels used herein also possess low compressive moduli. Thus neither the Rule of Mixtures, from general composites theory[12, 25], nor the semi-empirical Halpin-Tsai expression for fibrous composite materials[22] predict the observed increase in the compressive modulus for the multi-phase PEG hydrogels as compared to their single-phase counterparts. Briefly, these empirical formulations enable calculation of a composite material's modulus generally based on a weighted volume fraction of fibers and matrix. However both approaches limit the maximum achievable modulus of a composite material at the greatest moduli of the constituent phases. In other words, that the modulus achieved in the multi-phase materials in the present study far exceeds that of either individual phase implies that material structure, and not the material properties, is the main contributor to the greater moduli exhibited by the composite, multi-phase materials. Both phases thus must serve to counteract compressive loads.

While others have also observed substantial functional improvement when integrating fibers into a hydrogel matrix[13, 14, 60], the role of fibers oriented transverse to the direction of loading is underexplored. In articular cartilage, as an example, anisotropic collagen fibers are aligned parallel to the direction of externally applied compressive loads and anchor into the underlying zone of calcified cartilage. The hydrated GAGs and other extracellular matrix molecules largely bear compressive loads, while the collagen fibers resist tensile and shear [11, 57]. In contrast, the fibrous collagen scaffold networks in this study are generally isotropic and so are capable of resisting tensile loading in any direction. Accordingly, we observed that lateral expansion of the hydrogels under unconfined compression was reduced in the fiber-reinforced hydrogels compared to their non-reinforced counterparts. Given that each hydrogel has roughly equivalent initial diameter (and thus equivalent area), a greater force was required to load the hydrogels that incorporate the fibrous scaffold to an equivalent strain. This implies the fibrous scaffold contributes to stiffness by resisting lateral expansion of the hydrogels under applied compressive loads and leads to the higher modulus and toughness. While the compressive modulus of these fibrous collagen scaffolds is low, their tensile modulus is substantially greater (*e.g.*, ∼50 kPa in the hydrated state, compared

to a compressive modulus of ∼ 1.5 kPa)[9, 23, 56]. Moreover, the enhancement in mechanical properties with fiber reinforcement was more pronounced in the soft hydrogels, which is consistent with a higher lateral expansion observed in these materials. Thus, it can be deduced that the three-dimensional nature of the scaffold, which was carefully preserved during manufacture of the multi-phase materials, enabled axial compression to be translated into lateral strains that were limited by the fibers within the scaffold. In this manner, lateral expansion is reduced in the multi-phase scaffolds as the fibrous elements appear to be transversely loaded in tension. Thus both material (*i.e.*, properties of each constituent) and structural (*i.e.*, 3D geometry) contributions are critical factors in designing multi-phase materials for tissue engineering applications.

Bi-layer hydrogels, which are promising materials for osteochondral tissue engineering, [29, 36, 40, 49] were produced with a stiff layer to represent the ‘bone’ region, a soft layer to represent the ‘cartilage’ region, and a thin <100 μm, interface. The porous, fibrous scaffold was incorporated throughout the stiff, 30% (w/w) PEGDM layer and extended into the overlying soft, 10% (w/w) PEGDM by ∼500 – 1000 μm to simulate two critical architectures observed within the native osteochondral interface tissues: (1) a 3D collagen matrix within bone and (2) collagen fibrils that serve to anchor the soft hyaline cartilage to the underlying mineralized tissues. This design clearly does not recapitulate other key architectural attributes of the native tissues, such as the parallel-aligned collagen fibrils that form the structural backbone within hyaline articular cartilage[3] or the underlying mineralized tissues[11, 18]. Instead, we sought inspiration from the native osteochondral interface where collagen fibers extend from the zone of calcified cartilage through the hyaline cartilage to span tissues possessing moduli that vary by several orders of magnitude. These fibers thus serve as a physical anchor and bear loads such that they reduce stress concentrations that might otherwise form at the interface between the two tissues[11, 57, 55] Similarly, our material system enables us to evaluate the effectiveness of a fibrous phase to reduce stress and strain concentrations at the interface of two highly compliant, hydrated materials possessing dissimilar moduli.

A limitation of the present study, and a necessary component in future work, is the lack of experimental evaluation of shear failure of the interface between stiff and soft layers in bi-layered hydrogels[55]. In this study 17% of the single-phase, bi-layer hydrogels subjected to compressive loading exhibited a clear pattern of failure due to shear forces whereas none of the multi-phase materials failed in this manner. Such shear failure was noted by a circular fracture plane that was oriented ∼45° from the stiff-soft material interface and matched the plane of high intensity shear strains noted in FEM simulations (Fig. 6A).

The interface between soft and stiff layers in bi-layered hydrogels appeared to form a material continuum through which stresses and strains are transferred. This interface likely formed as a result of diffusion of the two adjacent hydrogels, thus creating physical entanglements between the two layers. Although high conversions are readily reached in these highly swollen networks, there is the potential for covalent bonds to form between the two layers as a result of incomplete conversion of the first layer. Similar to cartilage and bone that form the native osteochondral interface,[11, 57] the architecture of our bi-layer hydrogel leads to an abrupt change in mechanical properties across a relatively thin region.

For example, the tangent modulus of the stiff, mono-layer and single-phase hydrogels was ∼6.5× that of the soft hydrogels. In bi-layer hydrogels, the interface between the two layers was formed by a ∼70 um thick region that was formed by diffusion during polymerization. While this study did not directly evaluate properties within this interfacial region, this diffusional layer likely possessed a modulus in between that of the soft and stiff single-phase hydrogels. Further mechanical testing of this region, perhaps using atomic force microscopy, is needed to evaluate the modulus of this diffusional layer.

Observation and analysis of photographs and videos collected during compression testing (example in Fig. 5) clearly illustrated that the more compliant, soft hydrogel within the bi-layer experienced far greater deformation as compared to the stiff hydrogel layer under compressive loading. We hypothesized that inclusion of the fibrous scaffold would mitigate the stress and strain concentrations that result from loading at dissimilar interfaces joining fragile materials. Experimental evaluation of strains across the narrow interface region were not possible with our experimental setup. Therefore, computational finite element modeling (FEM) was used to evaluate how inclusion of the fibrous scaffold influenced stress and strain gradients across the interface and throughout each hydrogel layer. FEM indicated improved stress and strain profiles in bi-layered hydrogels with the inclusion of the fibrous scaffold. In the model, matched to experimental dimensions and test parameters, the fibrous scaffold penetrated 500 μm into the soft hydrogel layer. However some variability was likely inherent to our experimental fabrication process and the degree to which the sponge materials were swollen; consequently, penetration sometimes extended slightly beyond 500 μm. Unfortunately, these distances were not histologically evaluated as the samples were compressed to 40 % strain and often experienced failure after compressive strains exceeded 35 %, thus casting doubt on any subsequent physical analyses. For these reasons, the location and width of the fibrous scaffold within the hydrogel was not directly evaluated. However, visual assessment of these scaffolds indicated that the scaffold was centrally positioned (relative to the long axis of the sample) and spanned to less than 0.5 mm of each side of the hydrogel. No samples were included that deviated from these observations. However these manufacturing concerns proved to be minor. The coefficient of variance in experimental testing data was low, indicating small influence of any variability in scaffold penetration and construction of multi-phase materials. In addition, the FEM simulations demonstrated that the fibrous sponge largely improved stress and strain profiles across the interface. Additional FEM simulations demonstrated that increasing the penetration distance to 1000 μm resulted in further functional improvements. Overall, the fibrous scaffold appears to mitigate stress and strain distributions that would otherwise increase the propensity for interfacial failure between the dissimilar hydrogels.

Due to high lateral strains within the soft layer, no increase in modulus of bi-layer hydrogels was observed in experimental unconfined compression testing. However, FEM results predict that inclusion of the fibrous scaffold in bi-layered hydrogels contributes to a 4.16% greater compressive modulus at 20% strain. As the soft layer was observed to deform much more than the stiff layer in the bi-layered systems, it is likely that the stiff layer provided the major contribution to the modulus. Experimental compression testing also likely produced a mechanical response that was produced primarily by large compressive strains within the soft layer. Inclusion of the fibrous scaffold exerted little influence on this behavior as it

existed throughout the stiff layer and extended only a small distance into the soft layer. A different behavior was observed due to the assumptions used for the FEM simulations: *i.e.*, elastic material properties, linear stress-strain behavior, and a homogenized material where the hydrogel and fibrous scaffold moduli were summed (*i.e.*, similar to loading a rheological model containing two parallel springs). Thus, the constitutive relationships used for relating stress to strain in the FEM simulations may require modification to better match the observed behavior of the materials evaluated herein. Presently, experimental results from this study were implemented directly into the FEM to simulate each material region without specific constitutive material models. Additional materials testing is required to incorporate an appropriate phenomenological constitutive model into the FEM, such as the mean tensile modulus for the struts within the fibrous scaffold and lateral expansion data as a function of strain applied to the sample. Moreover, improvements to the FEM could include the hydrogel and the fibrous sponge as separate materials. This approach would permit valuation of how anisotropy and fiber orientation within a hydrogel matrix can be tailored to direct stress and strain gradients for specific functional applications. Last, while PEG hydrogels generally exhibit elastic behavior at low strains,[45] the high strains applied in this study resulted in non-linear stress-strain behavior. A range of strain energy functions exist that describe nonlinear behavior at high strains,[34] and optimization studies could be performed to ensure that the FEM is better able to accurately simulate behavior of all materials combinations in this study. While the FEM did not exactly simulate the observed experimental behaviors, the simulations generally represented the stress and strains produced by compressive loading of the material system under study. Refinement of this FEM to more closely represent experimental behaviors would enable its use in designing and optimizing new multi-phase and multi-layer materials for functional tissue engineering applications.

Conclusions

This study demonstrated the successful development of a hydrogel-based composite that informs the design of osteochondral tissue engineering applications. The integration of a relatively weak fibrous scaffold into a comparably weak hydrogel demonstrated vastly improved mechanical properties, where the structural nature of each material contributed to improved resistance to compression. Future studies will focus on evaluating how to capture similar functional improvements when an infiltrating fibrous scaffold is highly anisotropic, such as in functional tissue engineering of cartilage. Overall, this study establishes a new paradigm for osteochondral tissue engineering that has potential to be extended to regeneration of other soft tissue-to-bone interfaces and integrative soft tissue repair.

Acknowledgments

Research reported in this publication was partially supported by the University of Colorado Innovative Grant Program and NSF CAREER Award CBET #1055989 (K.R.C.K., A.N., M.S., V.L.F.); NSF CAREER Award DMR #0847390 (A.H.A., S.J.B.), NIH R21 AR063331 (L.C.M., B.A.C.H), and a NIH Pharmaceutical Biotechnology Training fellowship to A.H.A. Imaging experiments were performed in the University of Colorado Anschutz Medical Campus Advance Light Microscopy Core supported in part by NIH/NCATS Colorado CTSI Grant Number UL1 TR001082. The content is solely the responsibility of the authors and does not necessarily represent the official views of the NIH or NSF. The authors also thank Dr. Justine J. Roberts for assistance related to hydrogel synthesis and Rachael C. Paietta for contributions to mechanical testing methods and analysis.

References

1. Broom ND, Poole CA. A functional morphological-study of the tidemark region of articular-cartilage maintained in a non-viable physiological condition. Journal of Anatomy. 1982; 135:65–82. [PubMed: 7130057]
2. Bryant SJ, Bender RJ, Durand KL, Anseth KS. Encapsulating Chondrocytes in degrading PEG hydrogels with high modulus: Engineering gel structural changes to facilitate cartilaginous tissue production. Biotechnol Bioeng. 2004; 86:747–755. [PubMed: 15162450]
3. Bullough P, Goodfellow J. The significance of the fine structure of articular cartilage. J Bone Joint Surg Br. 1968; 50:852–857. [PubMed: 5706888]
4. Burdick JA, Anseth KS. Photoencapsulation of osteoblasts in injectable RGD-modified PEG hydrogels for bone tissue engineering. Biomaterials. 2002; 23:4315–4323. [PubMed: 12219821]
5. Caliari SR, Harley BA. Collagen-GAG scaffold biophysical properties bias MSC lineage choice in the presence of mixed soluble signals. Tissue Eng Part A. 2014; 20:2463–2472. [PubMed: 24568607]
6. Caliari SR, Harley BA. Structural and biochemical modification of a collagen scaffold to selectively enhance MSC tenogenic, chondrogenic, and osteogenic differentiation. Adv Healthc Mater. 2014; 3:1086–1096. [PubMed: 24574180]
7. Caliari SR, Mozdzen LC, Armitage O, Oyen ML, Harley BA. Award Winner in the Young Investigator Category, 2014 Society for Biomaterials Annual Meeting and Exposition, Denver, Colorado, April 16-19, 2014: Periodically perforated core-shell collagen biomaterials balance cell infiltration, bioactivity, and mechanical properties. J Biomed Mater Res A. 2014; 102:917–927. [PubMed: 24327556]
8. Caliari SR, Weisgerber DW, Grier WK, Mahmassani Z, Boppart MD, Harley BA. Collagen Scaffolds Incorporating Coincident Gradations of Instructive Structural and Biochemical Cues for Osteotendinous Junction Engineering. Adv Healthc Mater. 2015
9. Caliari SR, Weisgerber DW, Ramirez MA, Kelkhoff DO, Harley BA. The influence of collagen-glycosaminoglycan scaffold relative density and microstructural anisotropy on tenocyte bioactivity and transcriptomic stability. J Mech Behav Biomed Mater. 2012; 11:27–40. [PubMed: 22658152]
10. Campbell SE, Ferguson VL, Hurley DC. Nanomechanical mapping of the osteochondral interface with contact resonance force microscopy and nanoindentation. Acta Biomaterialia. 2012; 8:4389–4396. [PubMed: 22877818]
11. Carter DR, Beaupré GS, Wong M, Smith RL, Andriacchi TP, Schurman DJ. The mechanobiology of articular cartilage development and degeneration. Clinical Orthopaedics and Related Research®. 2004; 427:S69–S77. [PubMed: 15480079]
12. Chawla, KK. Composite Materials Science and Engineering. Springer; 2012.
13. Coburn J, Gibson M, Bandalini PA, Laird C, Mao HQ, Moroni L, Seliktar D, Elisseeff J. Biomimetics of the Extracellular Matrix: An Integrated Three-Dimensional Fiber-Hydrogel Composite for Cartilage Tissue Engineering. Smart Struct Syst. 2011; 7:213–222. [PubMed: 22287978]
14. Coburn JM, Gibson M, Monagle S, Patterson Z, Elisseeff JH. Bioinspired nanofibers support chondrogenesis for articular cartilage repair. Proc Natl Acad Sci U S A. 2012; 109:10012–10017. [PubMed: 22665791]
15. Cui W, Wang Q, Chen G, Zhou S, Chang Q, Zuo Q, Ren K, Fan W. Repair of articular cartilage defects with tissue-engineered osteochondral composites in pigs. Journal of Bioscience and Bioengineering. 2011; 111:493–500. [PubMed: 21208828]
16. Duan P, Pan Z, Cao L, He Y, Wang H, Qu Z, Dong J, Ding J. The effects of pore size in bilayered poly(lactide-co-glycolide) scaffolds on restoring osteochondral defects in rabbits. J Biomed Mater Res A. 2013
17. Farrell E, O'Brien FJ, Doyle P, Fischer J, Yannas I, Harley BA, O'Connell B, Prendergast PJ, Campbell VA. A collagen-glycosaminoglycan scaffold supports adult rat mesenchymal stem cell differentiation along osteogenic and chondrogenic routes. Tissue Eng. 2006; 12:459–468. [PubMed: 16579679]

18. Ferguson VL, Bushby AJ, Boyde A. Nanomechanical properties and mineral concentration in articular calcified cartilage and subchondral bone. J Anat. 2003; 203:191–202. [PubMed: 12924819]
19. Galperin A, Oldinski RA, Florczyk SJ, Bryers JD, Zhang MQ, Ratner BD. Integrated Bi-Layered Scaffold for Osteochondral Tissue Engineering. Advanced Healthcare Materials. 2013; 2:872–883. [PubMed: 23225568]
20. Gotterbarm T, Richter W, Jung M, Berardi Vilei S, Mainil-Varlet P, Yamashita T, Breusch SJ. An in vivo study of a growth-factor enhanced, cell free, two-layered collagen-tricalcium phosphate in deep osteochondral defects. Biomaterials. 2006; 27:3387–3395. [PubMed: 16488472]
21. Guo X, Liao J, Park H, Saraf A, Raphael RM, Tabata Y, Kasper FK, Mikos AG. Effects of TGF-beta 3 and preculture period of osteogenic cells on the chondrogenic differentiation of rabbit marrow mesenchymal stem cells encapsulated in a bilayered hydrogel composite. Acta Biomaterialia. 2010; 6:2920–2931. [PubMed: 20197126]
22. Halpin Affdl JC, Kardos JL. The Halpin-Tsai equations: A Review. Polymer Science and Engineering. 1976; 16:344–352.
23. Harley BA, Leung JH, Silva E, Gibson LJ. Mechanical characterization of collagen-glycosaminoglycan scaffolds. Acta Biomaterialia. 2007; 3:463–474. [PubMed: 17349829]
24. Harley BA, Lynn AK, Wissner-Gross Z, Bonfield W, Yannas IV, Gibson LJ. Design of a multiphase osteochondral scaffold III: Fabrication of layered scaffolds with continuous interfaces. Journal of Biomedical Materials Research Part A. 2010; 92A:1078–1093. [PubMed: 19301263]
25. Hashin Z, Shtrikman S. A variational approach to the theory of the elastic behaviour of multiphase materials. Journal of the Mechanics and Physics of Solids. 1963; 11:127–140.
26. Hortensius RA, Harley BA. The use of bioinspired alterations in the glycosaminoglycan content of collagen-GAG scaffolds to regulate cell activity. Biomaterials. 2013; 34:7645–7652. [PubMed: 23871542]
27. Im GI, Ahn JH, Kim SY, Choi BS, Lee SW. A hyaluronate-atelocollagen/beta-tricalcium phosphate-hydroxyapatite biphasic scaffold for the repair of osteochondral defects: a porcine study. Tissue Eng Part A. 2010; 16:1189–1200. [PubMed: 19883204]
28. Jiang CC, Chiang H, Liao CJ, Lin YJ, Kuo TF, Shieh CS, Huang YY, Tuan RS. Repair of porcine articular cartilage defect with a biphasic osteochondral composite. Journal of Orthopaedic Research. 2007; 25:1277–1290. [PubMed: 17576624]
29. Jin GZ, Kim JJ, Park JH, Seo SJ, Kim JH, Lee EJ, Kim HW. Biphasic nanofibrous constructs with seeded cell layers for osteochondral repair. Tissue Eng Part C Methods. 2014
30. Kandel RA, Grynpas M, Pilliar R, Lee J, Wang J, Waldman S, Zalzal P, Hurtig M, Team CBST. Repair of osteochondral defects with biphasic cartilage-calcium polyphosphate constructs in a Sheep model. Biomaterials. 2006; 27:4120–4131. [PubMed: 16564568]
31. Khanarian NT, Haney NM, Burga RA, Lu HH. A functional agarose-hydroxyapatite scaffold for osteochondral interface regeneration. Biomaterials. 2012; 33:5247–5258. [PubMed: 22531222]
32. Khanarian NT, Jiang J, Wan LQ, Mow VC, Lu HH. A hydrogel-mineral composite scaffold for osteochondral interface tissue engineering. Tissue Eng Part A. 2012; 18:533–545. [PubMed: 21919797]
33. Lee JC, Pereira C, Ren X, Huang W, Weisgerber DW, Yamaguchi DT, Harley BA, Miller TA. Optimizing collagen scaffolds for bone engineering: effects of crosslinking and mineral content on structural contraction and osteogenesis. Journal of Craniofacial Surgery. 2015
34. Lin DC, Shreiber DI, Dimitriadis EK, Horkay F. Spherical indentation of soft matter beyond the Hertzian regime: numerical and experimental validation of hyperelastic models. Biomechanics and Modeling in Mechanobiology. 2009; 8:345–358. [PubMed: 18979205]
35. Lin-Gibson S, Bencherif S, Cooper JA, Wetzel SJ, Antonucci JM, Vogel BM, Horkay F, Washburn NR. Synthesis and characterization of PEG dimethacrylates and their hydrogels. Biomacromolecules. 2004; 5:1280–1287. [PubMed: 15244441]
36. Lopa S, Madry H. Bioinspired Scaffolds for Osteochondral Regeneration. Tissue Eng Part A. 2014
37. Lu S, Lam J, Trachtenberg JE, Lee EJ, Seyednejad H, van den Beucken JJ, Tabata Y, Wong ME, Jansen JA, Mikos AG, Kasper FK. Dual growth factor delivery from bilayered, biodegradable hydrogel composites for spatially-guided osteochondral tissue repair. Biomaterials. 2014

38. Lynn AK, Best SM, Cameron RE, Harley BA, Yannas IV, Gibson LJ, Bonfield W. Design of a multiphase osteochondral scaffold. I. Control of chemical composition. Journal of Biomedical Materials Research Part A. 2010; 92A:1057–1065. [PubMed: 19301264]
39. Mente PL, Lewis JL. Elastic-modulus of calcified cartilage is an order of magnitude less-than that of subchondral bone. Journal of Orthopaedic Research. 1994; 12:637–647. [PubMed: 7931780]
40. Mohan N, Gupta V, Sridharan B, Sutherland A, Detamore MS. The potential of encapsulating “raw materials” in 3D osteochondral gradient scaffolds. Biotechnol Bioeng. 2014; 111:829–841. [PubMed: 24293388]
41. Moutos FT, Guilak F. Composite scaffolds for cartilage tissue engineering. Biorheology. 2008; 45:501–512. [PubMed: 18836249]
42. Nicodemus GD, Skaalure SC, Bryant SJ. Gel structure impacts pericellular and extracellular matrix deposition which subsequently alters metabolic activities in chondrocyte-laden PEG hydrogels. Acta Biomaterialia. 2011; 7:492–504. [PubMed: 20804868]
43. O'Brien FJ, Harley BA, Yannas IV, Gibson L. Influence of freezing rate on pore structure in freeze-dried collagen-GAG scaffolds. Biomaterials. 2004; 25:1077–1086. [PubMed: 14615173]
44. O'Brien FJ, Harley BA, Yannas IV, Gibson LJ. The effect of pore size on cell adhesion in collagen-GAG scaffolds. Biomaterials. 2005; 26:433–441. [PubMed: 15275817]
45. Roberts JJ, Earnshaw A, Ferguson VL, Bryant SJ. Comparative study of the viscoelastic mechanical behavior of agarose and poly(ethylene glycol) hydrogels. J Biomed Mater Res B Appl Biomater. 2011; 99:158–169. [PubMed: 21714081]
46. Roberts JJ, Nicodemus GD, Greenwald EC, Bryant SJ. Degradation Improves Tissue Formation in (Un)Loaded Chondrocyte-laden Hydrogels. Clinical Orthopaedics and Related Research. 2011; 469:2725–2734. [PubMed: 21347817]
47. Sharma B, Williams CG, Khan M, Manson P, Elisseeff JH. In vivo chondrogenesis of mesenchymal stem cells in a photopolymerized hydrogel. Plastic And Reconstructive Surgery. 2007; 119:112–120. [PubMed: 17255664]
48. Sherwood JK, Riley SL, Palazzolo R, Brown SC, Monkhouse DC, Coates M, Griffith LG, Landeen LK, Ratcliffe A. A three-dimensional osteochondral composite scaffold for articular cartilage repair. Biomaterials. 2002; 23:4739–4751. [PubMed: 12361612]
49. Shimomura K, Moriguchi Y, Murawski CD, Yoshikawa H, Nakamura N. Osteochondral Tissue Engineering with Biphasic Scaffold: Current Strategies and Techniques. Tissue Eng Part B Rev. 2014
50. Steinmetz NJ, Aisenbrey EA, Westbrook KK, Qi HJ, Bryant SJ. Mechanical loading regulates human MSC differentiation in a multi-layer hydrogel for osteochondral tissue engineering. Acta Biomaterialia. 2015
51. Vickers SM, Squitieri LS, Spector M. Effects of cross-linking type II collagen-GAG scaffolds on chondrogenesis in vitro: Dynamic pore reduction promotes cartilage formation. Tissue Engineering. 2006; 12:1345–1355. [PubMed: 16771647]
52. Villanueva I, Hauschulz DS, Mejic D, Bryant SJ. Static and dynamic compressive strains influence nitric oxide production and chondrocyte bioactivity when encapsulated in PEG hydrogels of different crosslinking densities. Osteoarthritis and Cartilage. 2008; 16:909–918. [PubMed: 18203631]
53. Wang DA, Williams CG, Yang F, Cher N, Lee H, Elisseeff JH. Bioresponsive phosphoester hydrogels for bone tissue engineering. Tissue Engineering. 2005; 11:201–213. [PubMed: 15738675]
54. Wang X, Wenk E, Zhang X, Meinel L, Vunjak-Novakovic G, Kaplan DL. Growth factor gradients via microsphere delivery in biopolymer scaffolds for osteochondral tissue engineering. J Control Release. 2009; 134:81–90. [PubMed: 19071168]
55. Wang Y, Meng H, Yuan X, Peng J, Guo Q, Lu S, Wang A. Fabrication and in vitro evaluation of an articular cartilage extracellular matrix-hydroxyapatite bilayered scaffold with low permeability for interface tissue engineering. Biomed Eng Online. 2014; 13:80. [PubMed: 24950704]
56. Weisgerber DW, Kelkhoff DO, Caliari SR, Harley BA. The impact of discrete compartments of a multi-compartment collagen-GAG scaffold on overall construct biophysical properties. J Mech Behav Biomed Mater. 2013; 28:26–36. [PubMed: 23973610]

57. Wong M, Carter DR. Articular cartilage functional histomorphology and mechanobiology: a research perspective. Bone. 2003; 33:1–13. [PubMed: 12919695]

58. Yannas IV, Lee E, Orgill DP, Skrabut EM, Murphy GF. Synthesis and characterization of a model extracellular matrix that induces partial regeneration of adult mammalian skin. Proc Natl Acad Sci U S A. 1989; 86:933–937. [PubMed: 2915988]

59. Yannas IV, Tzeranis DS, Harley BA, So PT. Biologically active collagen-based scaffolds: advances in processing and characterization. Philos Trans A Math Phys Eng Sci. 2010; 368:2123–2139. [PubMed: 20308118]

60. Yodmuang S, McNamara SL, Nover AB, Mandal BB, Agarwal M, Kelly TA, Chao PH, Hung C, Kaplan DL, Vunjak-Novakovic G. Silk microfiber-reinforced silk hydrogel composites for functional cartilage tissue repair. Acta Biomater. 2015; 11:27–36. [PubMed: 25281788]

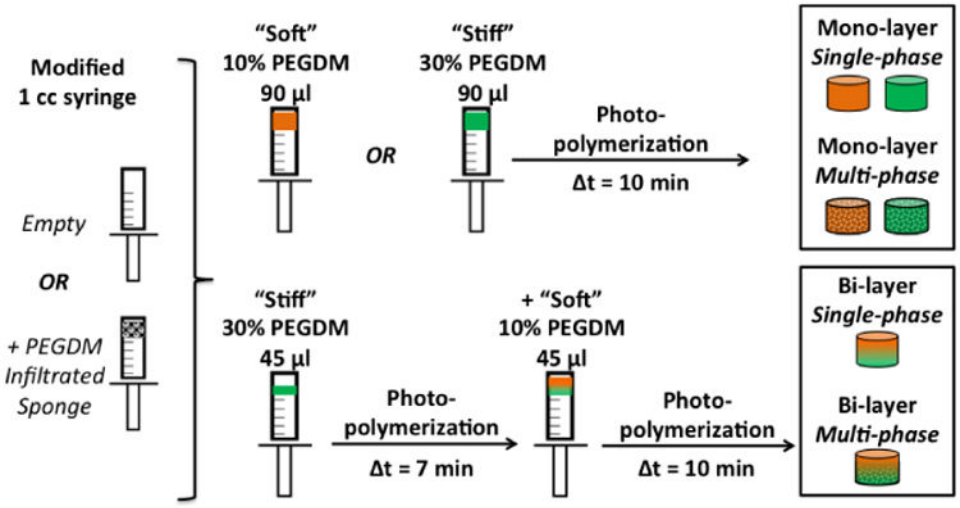

Figure 1.

Mono-layer hydrogels (height = 5 mm, diameter = 5 mm) were fabricated from soft 10% (w/w) or stiff 30% (w/w) PEGDM and bi-layer hydrogels consisted of a soft layer polymerized onto an underlying stiff layer of equivalent height (each layer height = 2.5 mm). Mono-layer hydrogels consisted of either hydrogel only (single-phase) or included a fibrous scaffold (multi-phase) that largely spanned the width and height of the construct. In the bi-layer hydrogels, the fibrous scaffold spanned the stiff layer and penetrated to ∼ 500 – 1000 μm into the soft layer.

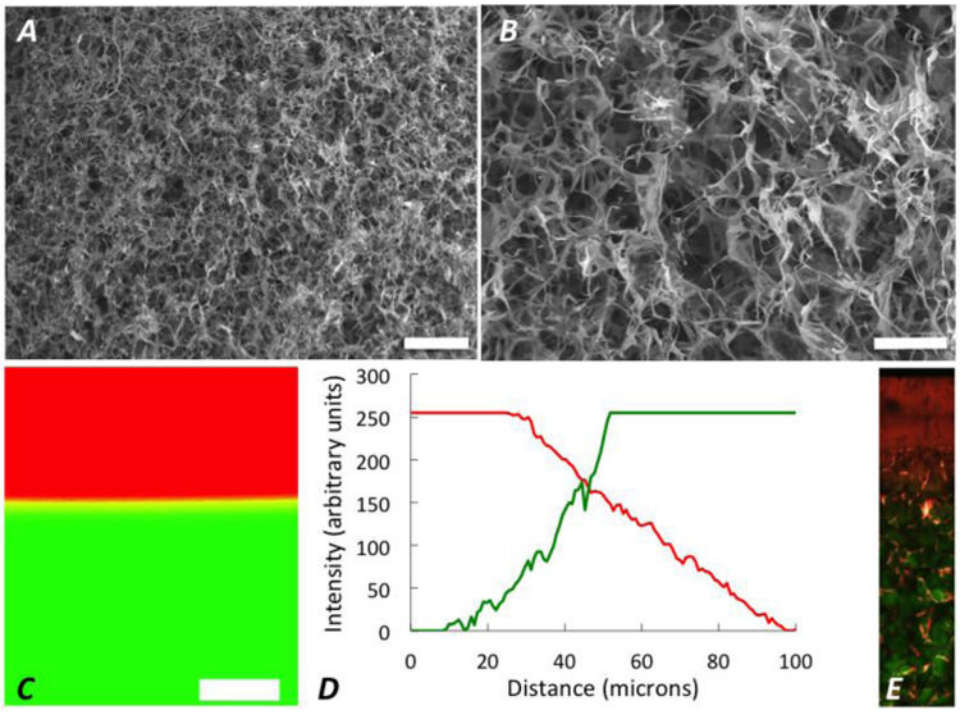

Figure 2.

30× (*A*; scale bar = 500 μm) and 90× (*B*; scale bar = 200 μm) SEM images of the fibrous scaffold, without any infilling hydrogel showing regularity, high porosity and continuity of the fibers throughout the scaffold as well as interconnected pore spaces. (*C*) A representative confocal microscopy image of the interface for a bi-layer hydrogel formed with a bottom layer from 30% PEGDM (green) and a top layer from 10% PEGDM (red) where the interface extends beyond the yellow band, and is denoted by the total distance across which both fluorophore channels detected fluorescence signal over the background; scale bar = 150 μm. The interface, a diffusional layer formed by mixing of the 10% (w/w) and 30% (w/w) PEGDM hydrogels, was evaluated to be 74 (16) μm as determined by the intensity; representative intensity plot in panel D. (*E*) 25× SHG image (Field Width = 359 μm) of the multi-phase, bi-layer hydrogel shows the 10% PEG (red) and 30% PEG (green) in pore spaces within the fibrous, collagen sponge (showing as pink due to image processing artifacts).

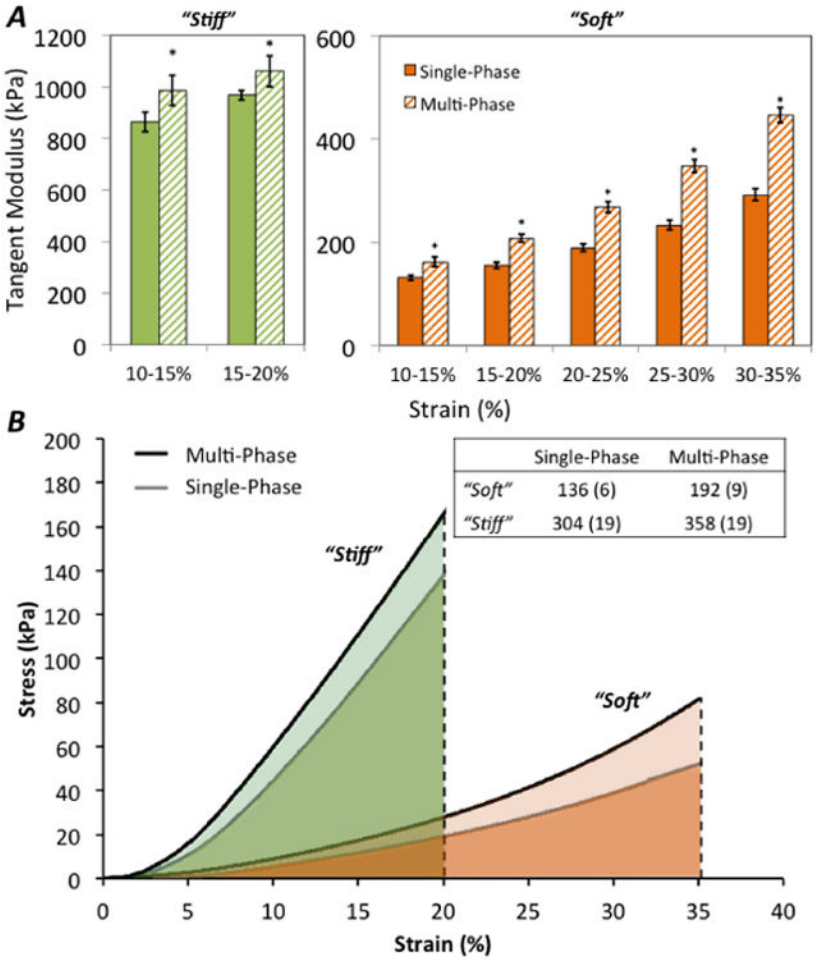

Figure 3.

Representative stress vs. strain plots for mono-layer, stiff (green) and soft (orange) hydrogels (A). Toughness was measured as the total area under each curve indicate to 20% strain for stiff constructs and 35% strain for soft hydrogels (B); inclusion of the fibrous scaffold imparted greater toughness for both stiff and soft multi-phase hydrogels. Table inset shows mean and (SD) for each material formulation.

* indicates statistically significant difference ($p < 0.05$) between single-phase vs. multi-phase for the same hydrogel formulation.

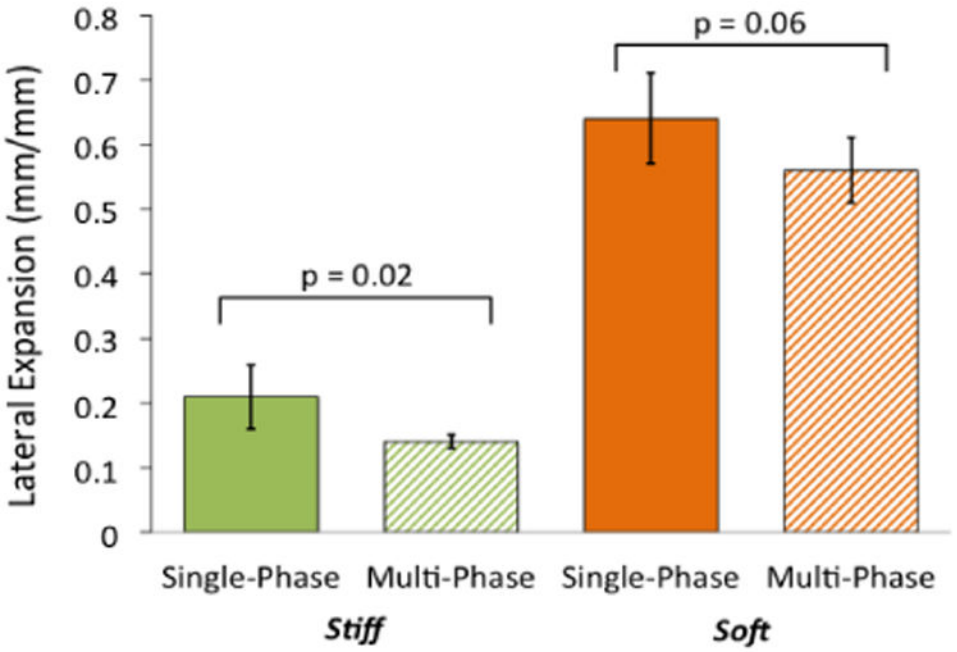

Figure 4.

Inclusion of a fibrous scaffold into multi-phase, mono-layer constructs reduced the lateral expansion under unconfined compressive axial loading in stiff (green) and soft (orange) as compared to single-phase, mono-layer constructs. Lateral expansion data are a ratio of the increase in sample width to the decrease in sample height and were measured at 40 % compressive strain.

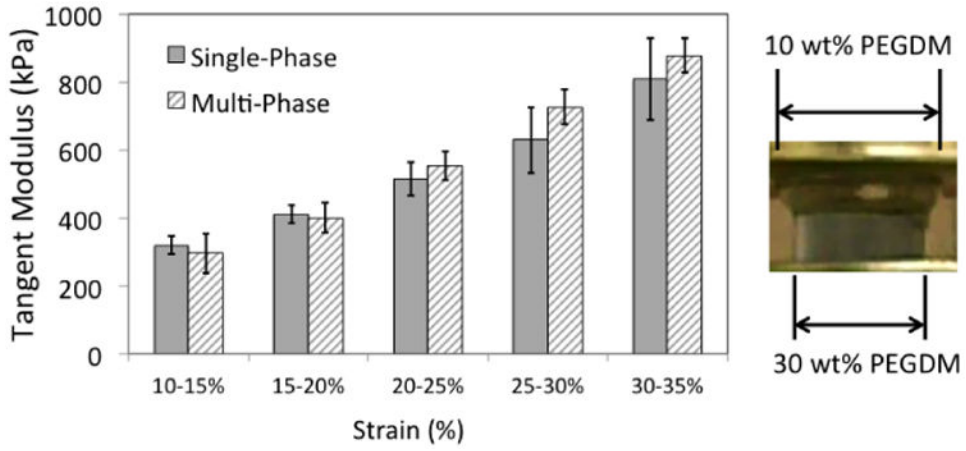

Figure 5.

Tangent modulus plotted vs. strain increment for single- and multi-phase, bi-layer hydrogels. No statistically significant differences were observed when including the fibrous scaffold within the bi-layer hydrogels (Left). The apparent similarities in measured tangent modulus likely resulted from the high expansion in the soft, 10% (w/w) PEG phase relative to the low expansion of the stiff, 30% (w/w) PEG layer (Right).

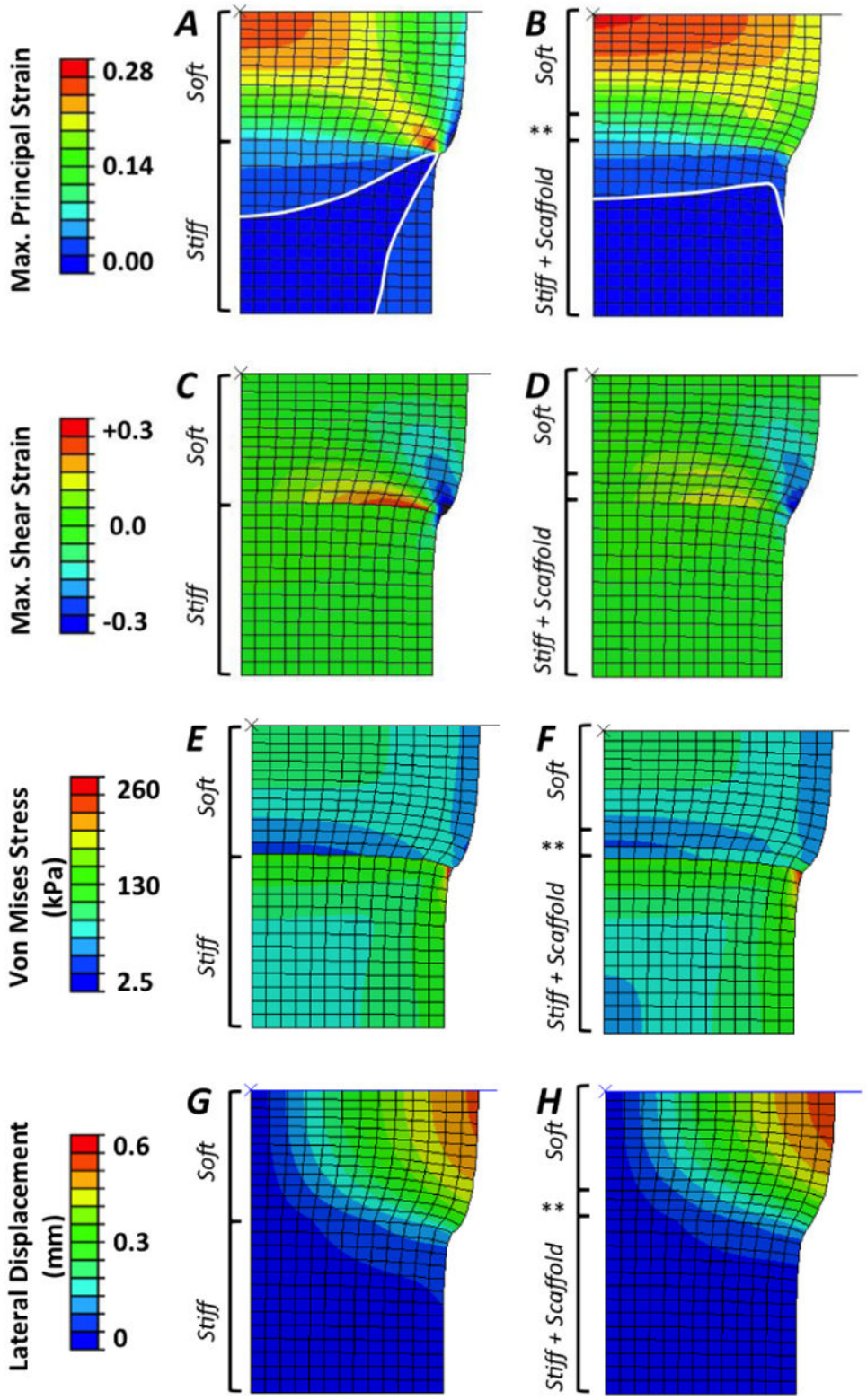

Figure 6.

Comparison of finite element modeling results for single-phase, bi-layer (Left Column) and multi-phase (hydrogel + fibrous scaffold; middle column) PEG hydrogels showing contour

plots of (A, B) maximum principal strain (note: stress contour between two lowest strain values are drawn to permit clear visualization), (C, D) maximum shear strain, (E, F) Von Mises stress (kPa), and (G, H) lateral displacement (mm). Finite element modeling shows a 4.2% increase in the compressive modulus of the bi-layered samples with inclusion of the fibrous scaffold throughout the stiff, 30% (w/w) PEG layer and penetrating 500 micrometers into the top, soft 10% (w/w) PEG layer (denoted by **).